ELSEVIER

Contents lists available at ScienceDirect

Earth and Planetary Science Letters

journal homepage: www.elsevier.com/locate/epsl





Assessing the feasibility of Distributed Acoustic Sensing (DAS) for moonquake detection

Qiushi Zhai ^{a,*}, Allen Husker ^{a,*}, Zhongwen Zhan ^a, Ettore Biondi ^a, Jiuxun Yin ^a, Francesco Civilini ^b, Luis Costa ^c

- ^a Seismological Laboratory, California Institute of Technology, Pasadena, California, CA, USA
- b NASA Goddard Space Flight Center, Greenbelt, MD, USA
- ^c Jet Propulsion Laboratory, California Institute of Technology, Pasadena, CA, USA

ARTICLE INFO

Keywords: Moonquake Distributed acoustic sensing DAS Lunar structure Scatter Fiber-optic seismology

ABSTRACT

Moonquakes can provide valuable insights into the lunar interior and its geophysical processes. However, extreme scattering of the lunar seismic waves makes seismic phase identification and source characterization difficult. In recent years, Distributed Acoustic Sensing (DAS) technology has emerged as a promising tool for seismic monitoring on Earth by turning a fiber optic cable into a dense array of strainmeters. DAS array can detect the full wavefield even in highly scattering environments and track scattered phases that were previously aliased on the standard sparse seismic networks. This study assesses the feasibility of DAS for moonquake detection. We present synthetic DAS recordings demonstrating its suitability for capturing moonquake signals in environments with significant scattering and low seismic velocities. By comparing Apollo moonquake signals with DAS's current minimum noise floor observed in Antarctica's quiet conditions, we find that existing DAS technology can detect more than 60 % of moonquakes previously recorded by Apollo seismic sensors. With expected and achievable improvements in DAS equipment, detection rates could surpass 90 %. Our findings suggest that DAS could, on average, detect around 15 moonquakes daily, with large fluctuations depending on recording during lunar sunrise/sunset for thermal moonquakes and the moon's distance from perigee/apogee for deep moonquakes. The deployment of DAS on the Moon could mark a revolutionary step in lunar seismology, significantly enhancing our understanding of the Moon's internal structure.

1. Introduction

Moon serves as an important window to Earth's early history, offering valuable insights into terrestrial planet formation and initial evolution (Cohen, 2020). The most effective, and often the only method to get detailed insights into the lunar crust, mantle, and core is through direct geophysical measurements such as seismic recordings. The profound importance of seismology has been demonstrated historically through the Apollo missions (Garcia et al., 2019; Goins et al., 1981; Toksöz et al., 1974) and more recently by the InSight mission to Mars (Lognonné et al., 2023). In lunar seismology, moonquakes are the key to studying the deep lunar interior. The seismic sensors deployed during the Apollo missions identified five primary types of seismic sources on the Moon: artificial and meteoroid impacts and thermal, shallow, and deep moonquakes (Civilini et al., 2023, 2021; Nakamura et al., 1981). Small and local events, typically comprising small impacts and thermal

moonquakes, offer valuable information about the Moon's shallow structure, including the surface regolith (a layer of loose rock and dust) and crust. In contrast, larger events, primarily deep moonquakes, shallow moonquakes, and significant impacts, are critical for investigating the deeper lunar layers. Thanks to the moonquake data captured by Apollo seismic sensors in the 1970s, our understanding of the Moon has significantly advanced (see references in Lammlein et al. (1974) and Garcia et al. (2019)). However, several critical questions remain unresolved (Cohen, 2020; Haviland et al., 2022; Kawamura et al., 2022). These include determining the size, state, and composition of the core, probing the properties of the lower mantle, unraveling the exact mechanisms behind shallow and deep moonquakes, understanding their distribution on the far side, and assessing potential risks they may pose to future lunar bases, etc.

The coming decade brings new opportunities to solve these unanswered lunar mysteries (Cohen, 2020; Haviland et al., 2022). Many

E-mail addresses: qzhai@caltech.edu (Q. Zhai), ahusker@caltech.edu (A. Husker).

^{*} Corresponding authors.

space agencies are planning crewed and uncrewed missions to the moon, including Artemis and Chang'e, alongside lunar base construction (Kawamura et al., 2022). These forthcoming missions present chances to install the next-generation seismic network on the lunar surface (Cohen, 2020; Haviland et al., 2022; Kawamura et al., 2022; Panning et al., 2020; Shearer, 2017; Weber et al., 2020). Determining the most suitable lunar seismic instruments is crucial (Nunn et al., 2020; Yamada et al., 2011) to unravel the outstanding questions that have not been answered by the Apollo seismic data. Recent initiatives like the Lunar Geophysical Network (LGN) (Haviland et al., 2022; Shearer, 2017), the Farside Seismic Suite (FSS) (Panning et al., 2021; Standley et al., 2023), and the Autonomous Lunar Geophysical Experiment Package (ALGEP) (Kawamura et al., 2022) propose the deployment of individual seismometers, including broadband stations (Haviland et al., 2022) and short-period seismometers (Nunn et al., 2019). Although these modern seismometers outperform those from the Apollo era, significant challenges persist. Particularly, analyzing the Moon's known strongly scattered seismic signals with individual seismometers is a significant challenge. Additionally, employing advanced array processing techniques in lunar seismology, such as beamforming and back projection, remains almost impossible with only a few individual seismometers far apart from each other.

Distributed Acoustic Sensing (DAS) is an emerging technology in seismology capable of transforming up to 100 kilometers of an optical fiber into a dense array of strainmeters, each spaced just a few meters apart (see references in Zhan (2019) and Lindsey & Martin (2021)). It is particularly suited for addressing the significant challenge of strong scattering in seismology (Atterholt et al., 2022; Yang et al., 2022b). By enabling array processing with thousands of channels (e.g., Li et al. (2023)), DAS opens a new window in lunar seismology. We believe DAS is an excellent candidate for instruments in next-generation lunar seismic networks to answer the unresolved critical scientific questions mentioned above (Cohen, 2020; Haviland et al., 2022; Kawamura et al., 2022). However, before deploying DAS on the moon, several engineering challenges must be addressed. These include deploying fiber on the Moon, providing power requirements during operation, and strategies for storing and transporting (either manually or through telemetry) data recorded by thousands of sensors. While these engineering challenges are critical, this paper focuses on a fundamental scientific question: Can DAS effectively detect various types of moonquakes? To address this, we undertake a structured analysis comprising the following four key steps. (1) We present real instances of moonquakes and earthquakes to illustrate DAS's advantages in addressing the strong scattering challenges inherent in lunar seismology. (2) Synthetic DAS signals are generated to investigate the influence of scatterers in the lunar subsurface, enhancing our understanding of their effects. (3) We convert existing Apollo moonquake data into strain rates. These are then compared against the minimum noise level of a DAS on Earth. Our following analysis includes evaluating the moonquake rate and the proportion of different moonquake types detectable above the minimum resolution of current and future DAS systems. (4) Various deployment scenarios for DAS on the moon are discussed, illustrating potential research opportunities with different combinations of operational duration and cable length.

${\bf 2.} \ \, {\bf Advantages} \ \, {\bf of} \ \, {\bf DAS} \ \, {\bf in} \ \, {\bf addressing} \ \, {\bf lunar} \ \, {\bf seismology} \ \, {\bf scattering} \ \, {\bf challenge}$

2.1. Apollo lunar seismic data and moonquakes

The moon is the only planetary body other than the Earth to have hosted seismic networks. The Passive Seismic Experiment (PSE) was equipped with seismometers at the Apollo 11, 12, 14, 15, and 16 landing sites, as shown in Fig. 1 (Nunn et al., 2020; Sutton and Latham, 1964). The Apollo 11 mission's seismometer had a brief operational life. The remaining sites, forming approximately a 1000 km-sided triangle, covered a significant area of the Moon's near side (the diameter of the moon is 3475 km). Particularly, Apollo 12 and 14 were less than 200 km apart, anchoring one corner of this triangular setup. All four stations were operating continuously from April 1972 to September 1977 (Nunn et al., 2020). Each PSE station was equipped with a vertical-component short-period sensor and a three-component mid-period sensor. The PSE mid-period seismometers had a flat instrument response from about 0.1 Hz to 1 Hz (Nunn et al., 2020; Sutton and Latham, 1964). For this study, we utilized data from the PSE seismometers at the Apollo 12, 14, 15, and 16 sites, excluding Apollo 11 due to its brief and non-overlapping operational period with other sensors (Fig. 1).

Apollo 17's Lunar Seismic Profiling Experiment (LSPE) brought 4 geophones (Fig. 1), configured in a roughly 100-meter triangular layout with an additional central unit (Haase et al., 2019; Kovach et al., 1973). The LSPE was only periodically activated after installation, with the

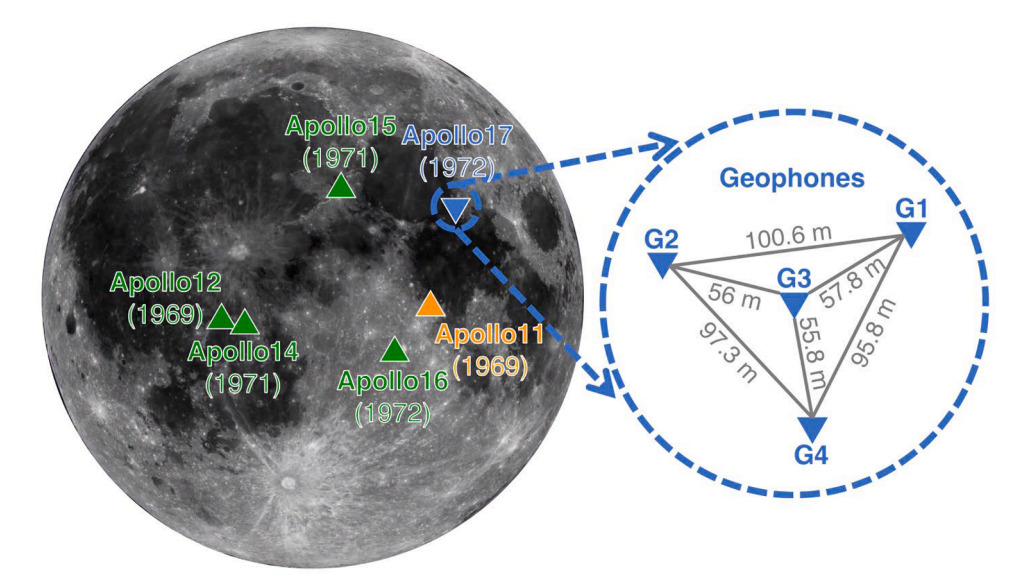


Fig. 1. Map of the Apollo seismic sensors on the lunar nearside. The Passive Seismic Experiments (PSE) seismometers were deployed at the sites of Apollo 11, 12, 14, 15, and 16. Note that the seismometer at the Apollo 11 site was operational for only one lunation. The Lunar Seismic Profiling Experiment (LSPE) geophones were deployed at the Apollo 17 site. This figure is adapted from Heffels et al. (2017), Nunn et al. (2020), and Civilini et al. (2023). The background image shows the lunar near side (Image Credit: NASA/Goddard Space Flight Center/Arizona State University).

longest period from August 1976 to April 1977 (Civilini et al., 2023). Each LSPE geophone included a single vertical-component short-period sensor. These geophones have their highest sensitivity range of roughly 4–30 Hz (Kovach et al., 1973). Nunn et al. (2020) provided a detailed reanalysis of the geophone instrument responses (Text S1).

The Apollo seismometers and geophones recorded thousands of moonquakes (Fig. 2) contributing significantly to our understanding of the lunar seismic activity (Civilini et al., 2023, 2021; Nakamura et al., 1981). These seismic events on the Moon originate from natural moonquakes and impacts. Moonquakes are categorized into three types: deep, shallow, and thermal. Deep moonquakes might be triggered by tidal stresses from Earth and the Sun (Lammlein et al., 1974; Latham et al., 1971; Turner et al., 2022). Shallow moonquakes could be tectonic events associated with young faults on the Moon (Watters et al., 2019). Thermal moonquakes, including natural thermal moonquakes and thermal moonquakes induced by the lunar module, primarily occur due to temperature changes at the lunar surface during lunar sunset and sunrise (Civilini et al., 2023, 2021; Duennebier and Sutton, 1974).

2.2. The pronounced scattering phenomenon in lunar seismology

Lunar seismic signals are characterized by emergent arrivals (long time between first arrival and peak ground movement), significant scattering, and very long decay times, distinguishing them markedly from the generally well-defined P & S phases on Earth (Fig. S1). The Apollo stations' digitizers recorded these signals at low resolutions with high bit noise (Kovach and Watkins, 1973; McAllister et al., 1969; Nunn et al., 2020). Bit noise, the erratic fluctuation of the least significant bit, was a notable issue with these digitizers. These two aspects have made finding phases in the Apollo seismic waveforms very difficult, because the first arrival slowly emerges out of the bit noise and the coda from the first arrival envelops later arrivals that are also emergent. This also makes it difficult to measure the time of the end of the waveform.

This scattering challenge was particularly highlighted by the Lunar Seismic Profiling Experiment (LSPE) during Apollo 17 (Fig. 1). The four LSPE geophones detected thousands of thermal events, attributed to daily temperature changes (Civilini et al., 2023). However, it is not possible to identify phases or packets within the wave train that correspond between the geophones, and even the exact first arrivals of events are difficult to determine (Civilini et al., 2023). Consequently, these limitations make the accurate localization of thermal moonquakes impossible. Only the direction of wave origin (back azimuth) from the geophone array is measurable (Civilini et al., 2023, 2021). Fig. 3a-b shows one of the largest seismic signals recorded at the geophones, highlighting the differences between the signals captured by two geophones, only 100 m apart (Fig. 1). This example underlines the inherent

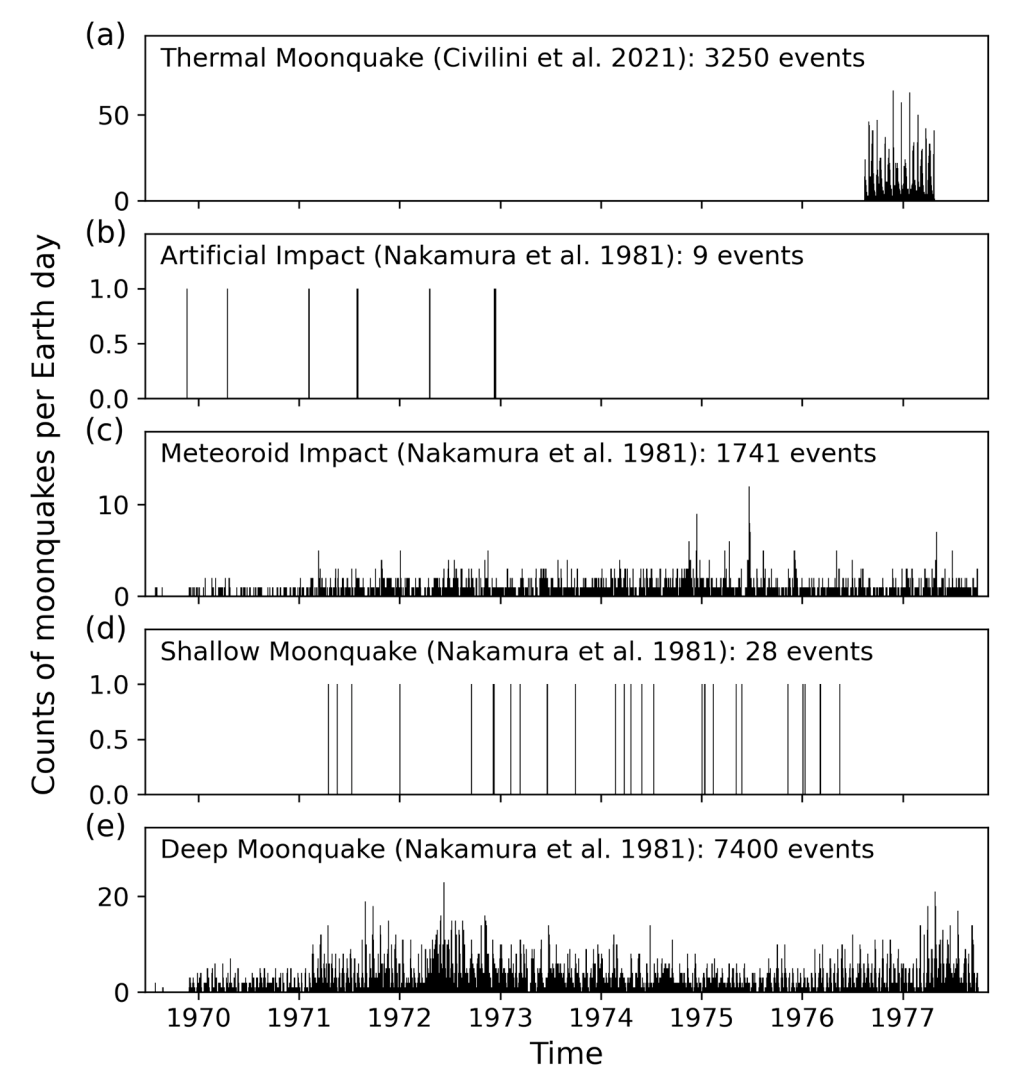


Fig. 2. Daily counts of moonquakes recorded by the Apollo seismic sensors. The top subfigure presents the (a) thermal moonquakes detected by the geophones of Apollo 17 (Civilini et al., 2023, 2021). The remaining four subfigures display (b) artificial impacts, (c) meteoroid impacts, (d) shallow moonquakes, and (e) deep moonquakes as recorded by the seismometers of Apollo 12, 14, 15, and 16 (Nakamura et al., 1981).

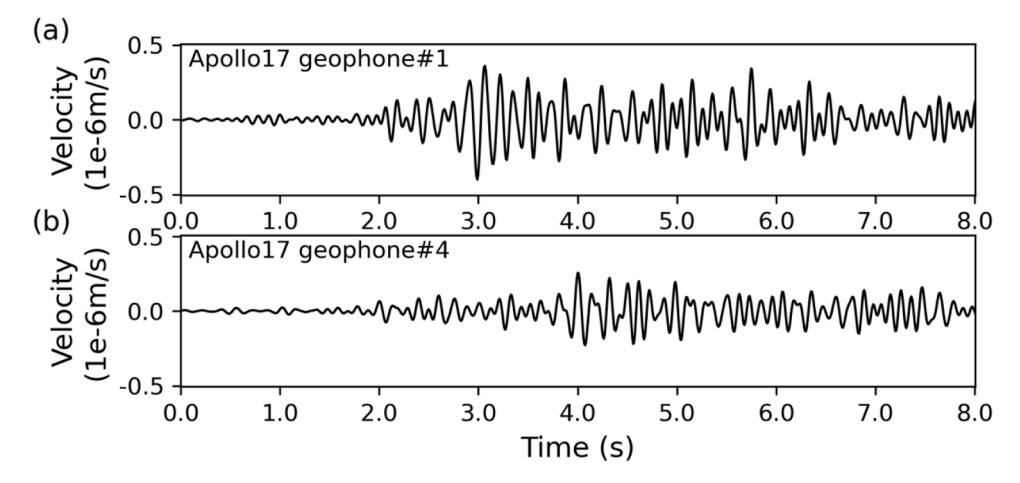


Fig. 3. Examples of observed signals of scattered wave fields of moonquakes. (a) The waveform of a thermal moonquake (1976–10–03T19:30:12 UTC) recorded on the Apollo 17 geophone#1 (Fig. 1). (b) The waveform of the same event as it is in (a) but recorded on geophone#4, which is about 100 m apart from geophone#1 (Fig. 1).

difficulty in matching phases or determining the exact initial arrival across seismometers on the Moon due to the scattering.

In addition to moonquake source analysis, the Moon's intense scattering effect poses significant challenges in studying the moon's structure. For example, Apollo 17 astronauts deployed explosives to generate seismic sources for the LSPE array to characterize the local seismic velocity structure (Cooper et al., 1974). Despite using known sources, the uncertainty in the first arrival is so large that a series of papers has reanalyzed the same data multiple times, resulting in changes to the identified phases, number of layers, and the inferred velocity structures (Cooper et al., 1974; Cooper and Kovach, 1975; Haase et al., 2019; Heffels et al., 2017; Kovach et al., 1973; Kovach and Watkins, 1973). Velocity measurements in the top few meters varied widely, ranging from 100 m/s to 327 m/s using the active source. Other attempts that used the scattered wavefield in the coda of moonquakes found even slower seismic velocities, in the tens of meters per second range, suggesting these were surface wave measurements (Larose, 2005; Sens-Schönfelder and Larose, 2010).

Beyond the difficulties in studying the Moon's shallow layers, the pronounced scattering effect presents significant challenges in understanding its deep structure and deep moonquakes. A fortunate aspect of deep moonquakes is their tendency to occur in clusters as repeating sources. This characteristic has enabled researchers to utilize seismogram stacking to identify seismic phases (Bulow et al., 2005; Nakamura, 2005). However, when comparing the stacked data from various studies, discrepancies emerge. Notably, stacks presumed to be from the same repeating sources often show low correlation coefficients when cross-compared in independent analyses (Nunn et al., 2020). The observed inconsistencies in the stacked data suggest potential misalignments and raise doubts about the accuracy of the identified seismic phases, implying that they may have been incorrectly interpreted in these cases.

Leveraging abundant, high-quality seismic data on Earth has advanced our understanding of Earth's scattering phenomena (Atterholt et al., 2022; Nielsen and Thybo, 2006; Yang et al., 2022b). For instance, the scattering of high-frequency oceanic Pn and Sn waves suggests that heterogeneities in Earth's lithosphere exhibit longer horizontal correlation distance than vertical (Kennett and Furumura, 2013). In contrast, knowledge of scattering on the Moon remains constrained by the low-resolution data from Apollo missions. To address the unresolved scientific questions left by Apollo data, next-generation seismic instruments for lunar deployment must be carefully designed. These instruments should overcome known challenges, particularly the Moon's strong scattering effects, a task not readily achievable by simply updating Apollo seismometers to modern seismometers or deploying

mini arrays of seismometers (Fig. 3).

2.3. Advantages of DAS in highly scattering seismic environments

DAS can convert a fiber optic cable into a dense array of thousands of strainmeters over a short distance. This innovative technology employs interferometry of backscattered light passing through the cable to find femtosecond changes in arrival time that come from changes in strain along the cable (Lindsey and Martin, 2021; Zhan, 2019). Each DAS channel functions as a longitudinal strainmeter. The channel spacing can be finely tuned, ranging from several meters to less than a meter, forming a dense seismic array. This capability has significantly advanced our understanding of Earth's structure and earthquake physics (Ajo-Franklin et al., 2019; Li et al., 2023; Martin et al., 2017; Spica et al., 2020; Yang et al., 2022a; Zhai et al., 2024), and proven effective in extreme environments like submarine (Williams et al., 2019), volcanic (Biondi et al., 2023; Jousset et al., 2022), and glacial settings (Walter et al., 2020).

DAS stands out as a highly effective tool for addressing the significant scattering issues encountered in seismology, with the potential to revolutionize lunar seismic studies. Fig. 4a-c demonstrates the ability of DAS to correlate the seismic waveform from a local earthquake near Ridgecrest, CA. Some highly scattered parts of the waveform, generated by faults across the array, are highlighted in Fig. 4b-c (Atterholt et al., 2022; Yang et al., 2022b). Unlike individual seismograms which struggle to correlate waveforms in such environments (as shown in Fig. 4d-e, similar to moonquake signals in Fig. 3), DAS leverages the complete data from the cable to clearly present the coherent wavefield in scattered regions (Fig. 4c). This suggests that even cables a few hundred meters long can provide invaluable data unobservable by standalone seismometers.

DAS measures strain or strain rate along the fiber optic cable. Theoretically, this means that DAS can efficiently measure seismic phases, such as surface waves, that travel parallel to the cable's orientation. Although theoretically less sensitive to waves arriving perpendicular to the cable, DAS has successfully measured nearperpendicularly arriving P and SV phases from teleseismic earthquakes (Yu et al., 2019), as depicted in Fig. 5. This figure showcases a teleseismic P wave recorded by DAS, arriving almost perpendicular to the surface and distinctly visible in the data. The clear visibility of these teleseismic P waves is attributed to near-surface scattering. In Fig. 5b, the "inverted-V" shaped patterns indicate scattered phases originating from strong heterogeneities near the surface. The slope of these "inverted-V" shapes reveals the velocity near the surface. Notably, these scattered phases propagate more slowly than the initial planar P wave

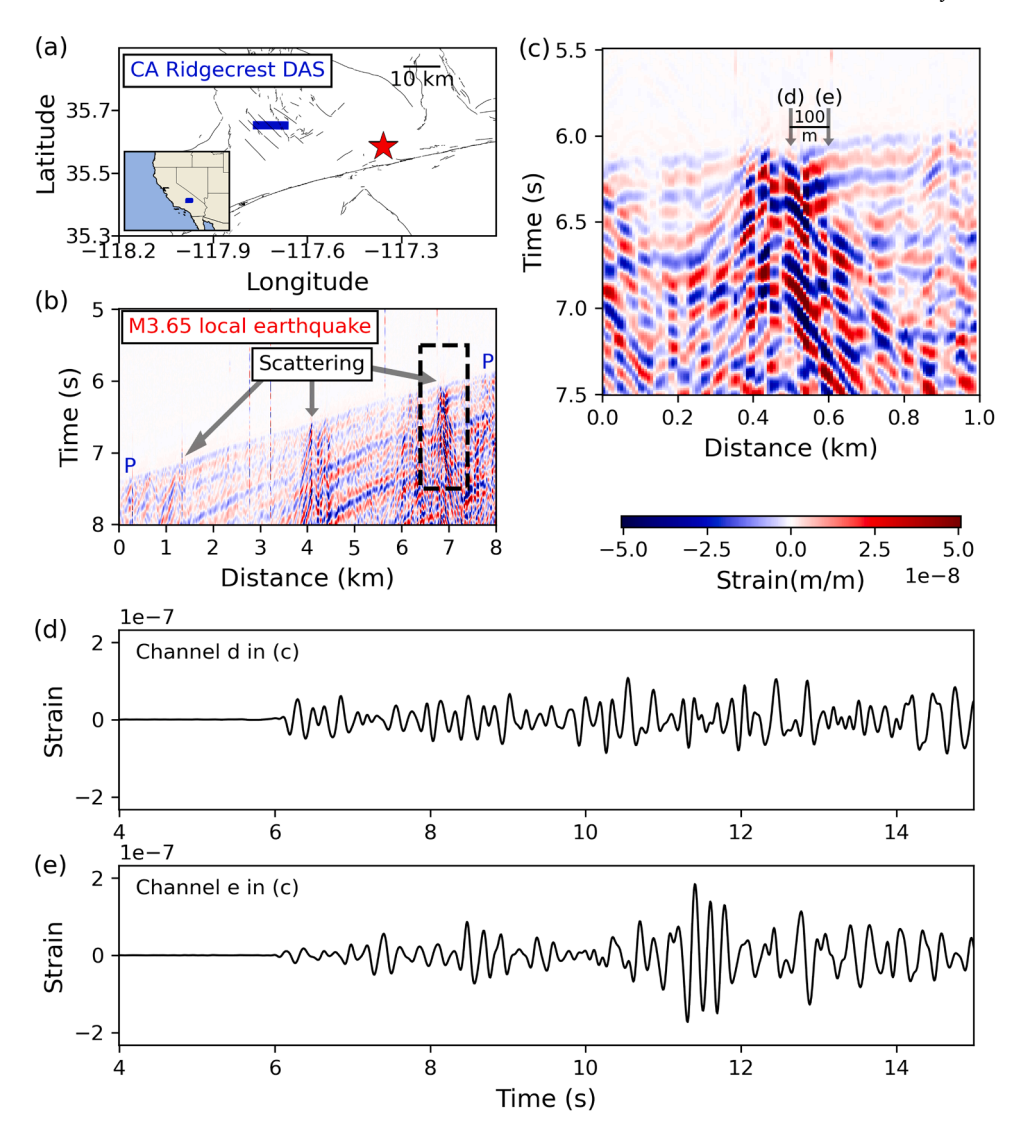


Fig. 4. Example of a local earthquake recorded on a DAS array in CA. (a) shows a DAS array in Ridgecrest, CA, and a local earthquake (red star), 07/19/2019, 10:47:05.4 UTC, M3.65, Latitude: 35.585, Longitude: -117.35783, Depth: 4.6 km. Distance: 33.2 km. (b) is the waveform of the local earthquake in (a) recorded by the CA Ridgecrest DAS. (c) is a scattered part of the waveform, a zoom into the dashed box in (b). (d-e) are examples of two individual DAS channels located 100 m apart, similar to Fig. 3a-b.

(Fig. 5b). It suggests that DAS can effectively detect plane wave arrivals perpendicular to the cable by capturing the scattered surface waves (Fig. 5b) that travel parallel to the cable. Consequently, for DAS data conversion between strain rate and acceleration, we can use the seismic velocity of the scattered surface waves (Fig. 5b) rather than the apparent velocity of the teleseismic body wave.

3. Evaluating moonquake detectability with DAS

While DAS has proven effective in capturing seismic signals in Earth's harsh environments and offers promising solutions to the Moon's scattering issues, it is essential to acknowledge its current limitations. DAS detects signals through its single horizontal components, making it less effective in directly capturing body waves. This characteristic raises questions about its ability to detect deep moonquakes and teleseismic moonquakes, where body-wave arrivals are perpendicular to the horizontal orientation of the DAS cable. Part of this concern has been addressed in the previous section (Fig. 5b). However, a more detailed understanding of scattering effects on DAS recordings is still needed. Additionally, DAS tends to exhibit higher instrumental noise compared to modern broadband seismometers (Lindsey and Martin, 2021; Zhan,

2019), particularly at low frequencies. This aspect of DAS technology introduces doubts regarding its capacity to detect moonquakes. In this section, we aim to rigorously evaluate the capability of DAS in moonquake detection. To achieve this, we will analyze synthetic DAS data and actual data from Apollo lunar seismic recordings alongside DAS recordings obtained on Earth. This comprehensive approach will provide a clearer understanding of DAS's effectiveness and limitations in detecting moonquakes.

3.1. Generating synthetic DAS signals for moon near-surface scattering analysis

To illustrate how the near-surface heterogeneities affect the recordings of strain measured by a surface-deployed DAS cable, we perform four different simulations (Fig. 6, Fig. S2, and Fig. S3) using an elastic isotropic finite-difference approximation (Biondi, 2021). We apply a free-surface boundary condition on the top part of the model and absorbing layers in the other sections of the domain (Robertsson, 1996). The velocity model (Fig. S2) is described in Heffels et al. (2017), which presents a shallow velocity layer with seismic velocities of 100 m/s. Spatial sampling in all synthetic experiments was set at 2 m, with a

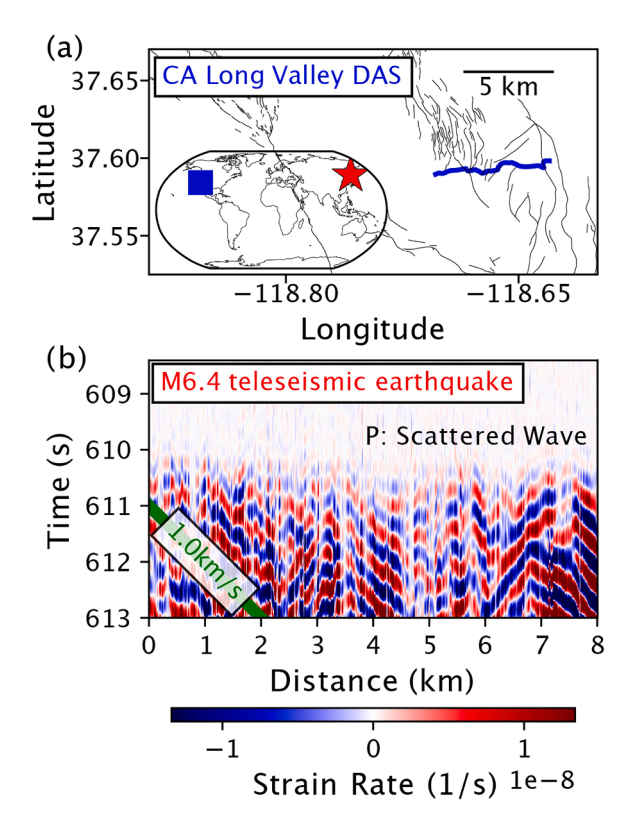


Fig. 5. Example of a teleseismic earthquake recorded on a DAS array in CA. (a) shows a DAS array at Long Valley, CA, and a teleseismic earthquake (red star), 11/30/2020, 22:54:34.6 UTC, Mw 6.4, Latitude: 140.7971, Longitude: 48.2521, Depth: 589 km. Distance: 69 degrees. (b) is the teleseismic direct P wave and the following scattered wave of the earthquake in (a) recorded by CA Long Valley DAS. The green line shows a reference wave speed of 1.0 km/s.

vertically propagating compression wave injected from the bottom. The simulations feature a source with a dominant frequency of 2 Hz. To mimic the presence of near-surface scatterers, we introduce Gaussian anomalies whose size follows a lognormal distribution with velocity variations uniformly distributed between –5% and 5% (Toksöz et al., 1974). The simulation of the near-surface scattering behavior is comparable to the synthetic scenario considered by Wu et al. (2024), which is based on the empirical observations of moonquake coda waves (Blanchette-Guertin et al., 2012; Dainty et al., 1974; Gillet et al., 2017). Additional details on the simulation parameters can be found in Text S2.

Our synthetic waveform tests (Fig. 6 and Fig. S3) demonstrate DAS's capability to effectively detect deep moonquakes. In scenarios without scatterers, a DAS cable does not record a P wave incident perpendicular to the cable (Fig. S3a). However, as the number of scatterers increases, so does the energy conversion from the original vertical P wave to horizontal motion, thus amplifying the strain rate detected by DAS (evident from the increasing amplitude in Fig. S3, panels a to d). This means that we could use what is typically a perceived disadvantage (the scatterers, Fig. 6a) and have it be an advantage in future lunar seismology with DAS. Prominent scatterers (Fig. 6a) allow for the observation of scattered phases in the DAS recordings, forming "inverted-V" shapes over extended durations (Fig. 6b). The slope of these scattered phases corresponds to the velocity of the upper layer, akin to observations in Californian DAS arrays (Figs. 4 and 5). Although DAS strain rate seismograms taken only 100 m apart show no clear coherency (Fig. 6cd), DAS's all-channel recordings effectively reveals the propagating scattered waves, displaying constructive and destructive interference within individual seismograms, similar to measurements in California (Figs. 4 and 5). Our synthetic DAS recordings highlight DAS's suitability for detecting seismic activity in highly scattered environments with low

seismic velocities, conditions that closely resemble the lunar near-surface.

3.2. Comparing Apollo moonquake signals with the Earth-based DAS noise level

To evaluate the capability of DAS in detecting moonquakes, we compare moonquake data recorded by Apollo seismometers and geophones with the DAS noise level obtained on Earth. The terrestrial DAS data were from the South Pole, selected due to its minimal anthropogenic noise, particularly during times when the Amundsen-Scott South Pole Station is less active, such as local weekends (Anthony et al., 2021). This site serves as an effective terrestrial analog for the Moon's quiet seismic environment.

DAS technology measures strain or strain rate along a fiber optic cable, contrasting with the displacement, velocity, or acceleration measurements typical of seismometers. The strain rate is equal to acceleration divided by the apparent velocity along the DAS cable $(\dot{\epsilon}=-\ddot{u}/c)$ (Yu et al., 2019). Given this difference in measurement parameters, our analysis involves several key steps: (1) Conversion of Apollo seismometer and geophone data, originally recorded in terms of velocity, into strain rates. (2) Transformation of these time-domain strain rates from moonquake signals into the frequency domain. (3) Calculation of the noise level spectrum of the DAS strain rate recorded in Antarctica. (4) Comparative analysis between the spectral profiles of moonquake signals and the DAS noise level. Through these steps, we aim to comprehensively assess the feasibility and efficiency of DAS in detecting moonquakes as compared to conventional Apollo seismometers.

3.2.1. Converting the Apollo lunar seismic data to strain rate

We analyze all the moonquakes recorded by the PSE and the LSPE listed in the catalogs of Nakamura et al. (1981) and Civilini et al. (2023). The seismic data were first cut to windows around the arrivals of moonquakes (Fig. 7a). We removed the mean and linear trend, and then tapered and despiked the raw PSE and LSPE data. The data were then converted to acceleration using the instrument response file from the supporting information in Nunn et al. (2020). This conversion from acceleration to strain rate depends on the apparent velocity as previously detailed in Section 2.3. The latest velocity model of the lunar crust has a velocity of about 300 m/s for the upper 250 m and 1000 m/s below that (Heffels et al., 2017). The lunar regolith, approximately a 10-meter thick unconsolidated surface layer, has velocities ranging between 30 m/s and 50 m/s (Civilini et al., 2023; Larose, 2005; Sens-Schönfelder and Larose, 2010). In this study, we have assumed a conservative velocity of 300 m/s to estimate DAS measurements in strain rate for all moonquakes. This assumption is based on the scattered waves at the lunar surface traveling at speeds in the tens of meters per second (Civilini et al., 2023; Larose, 2005; Sens-Schönfelder and Larose, 2010). In the supplementary material (Fig S4, Fig S5, and Table S1), we undertake a comparable analysis for the case of an apparent wave speed of 1000

3.2.2. Spectral analysis of Apollo moonquake waveforms in strain rate

The digitizers used for the PSE and the LSPE were very low-resolution with high bit noise, recording data at 10 and 7 bits, respectively (Kovach and Watkins, 1973; McAllister et al., 1969; Nunn et al., 2020). Although modern digitizers with oversampling techniques largely mitigate this problem, the significant bit noise present in many moonquake recordings suggests that it was a substantial contaminant of the true seismic signal in the Apollo data (Kovach and Watkins, 1973; McAllister et al., 1969; Nunn et al., 2020). Owing to the significant bit noise in the digitizer data, the conventional practice of transforming waveforms from the time domain to the frequency domain using a Fourier transform was deemed unsuitable for this study.

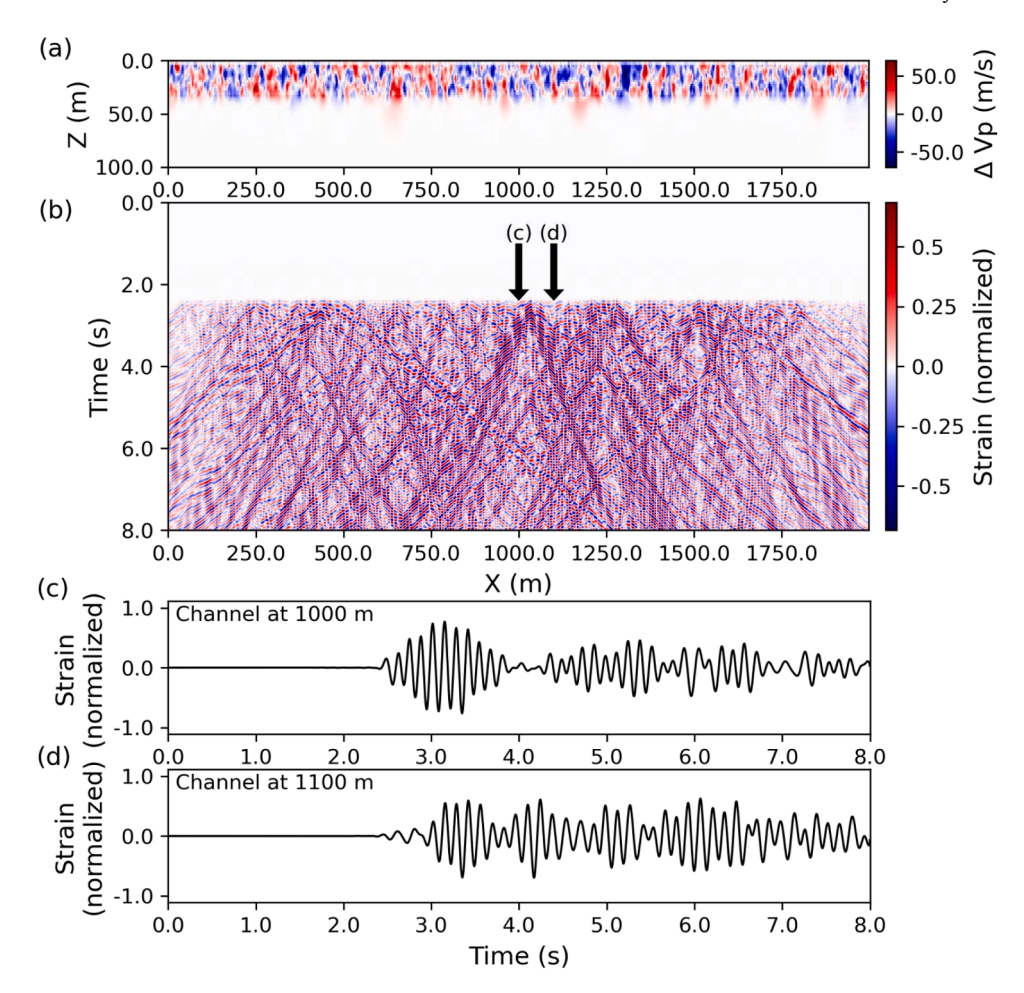


Fig. 6. Example of DAS synthetics with scatterers in moon near-surface. (a) The velocity pattern that arises from the random distribution of scatterers. (b) The equivalent of what is measured on DAS, similar to Fig. 4c. (c) and (d) Two seismograms of the strain measured at two places 100 m apart on the DAS, similar to Figs. 3a-b and 4d-e. DAS synthetics using different distributions of scatterers can be found in Fig. S3.

To address these challenges, we employed narrow-band filtering in the time domain, which allowed us to accurately assess the frequency content of the recorded signals without the interference of the bit noise (Clinton and Heaton, 2002). Fig. 7a demonstrates this technique using an octave-wide narrow bandpass filter on a moonquake recording. For each bandpass, the peak strain rate was identified and plotted against the central frequency of the band for all moonquakes (Fig. 7b-f). This approach prevented the incorporation of bit noise into the spectral analysis and eliminated the arbitrariness associated with selecting the window length, thus ensuring a cleaner spectral representation where the peak amplitude reliably exceeds the noise level (Clinton and Heaton, 2002).

3.2.3. Spectral analysis of the noise level of DAS strain rates in Antarctica In this study, DAS data from Antarctica is utilized for comparison with the Apollo seismic data. The Antarctic environment, noted for its low noise, is the Earth's closest analog to the lunar surface. The DAS system was set up along a fiber optic cable running between the South Pole Remote Earth Science and Seismological Observatory and the Amundsen-Scott South Pole Station. The chosen data encompasses a quiet period of half an hour on a Sunday afternoon at the South Pole, dated January 8, 2023. This particular DAS array consists of 8000 channels with a 1-meter channel spacing and a gauge length of 8.17 m (the length of the fiber optic segment over which the system averages the measurements).

To determine the DAS minimum resolution (yellow dashed line in Fig. 7b-f), we adopted the approach used by Clinton and Heatonn

(2002), which was originally employed to assess the Peterson Low Noise Model (Peterson, 1993). This involves computing the power spectral density (PSD) of each channel via a fast Fourier transform. The resultant frequency-dependent root mean square (RMS) curve for each channel is then calculated from its PSD, aligning with the octave-wide narrow bandpass range applied to the moonquake data. The average minimum resolution of the DAS array is calculated by taking the median of these RMS curves across all channels.

Acknowledging ongoing advancements in DAS technology, we anticipate further improvements in signal detection capabilities. Innovations include engineered fiber optic cables with enhanced backscattering or point reflectors (Westbrook et al., 2023) and multi-frequency interrogation architectures, aimed at increasing optical signal-to-noise-ratio, robustness against signal fading and non-linearity during multi-frequency interrogation (Ogden et al., 2021), as well as developments in frequency-stabilized lasers (Jeon et al., 2023) and advanced post-processing techniques (Vidal-Moreno et al., 2022) aimed at improving low-frequency noise and long-term signal stability. For example, Han et al. (2021) show that the acoustic sensitivity has been significantly improved by ~10 times by using a novel sensitivity-enhanced optical cable. Reflecting these technological strides, we also present an alternative reference DAS noise level (represented by the green dashed line in Fig. 7b-f) that is projected to be 10 times lower than the current South Pole DAS noise level. This serves as a benchmark for potential technological enhancements in the coming vears.

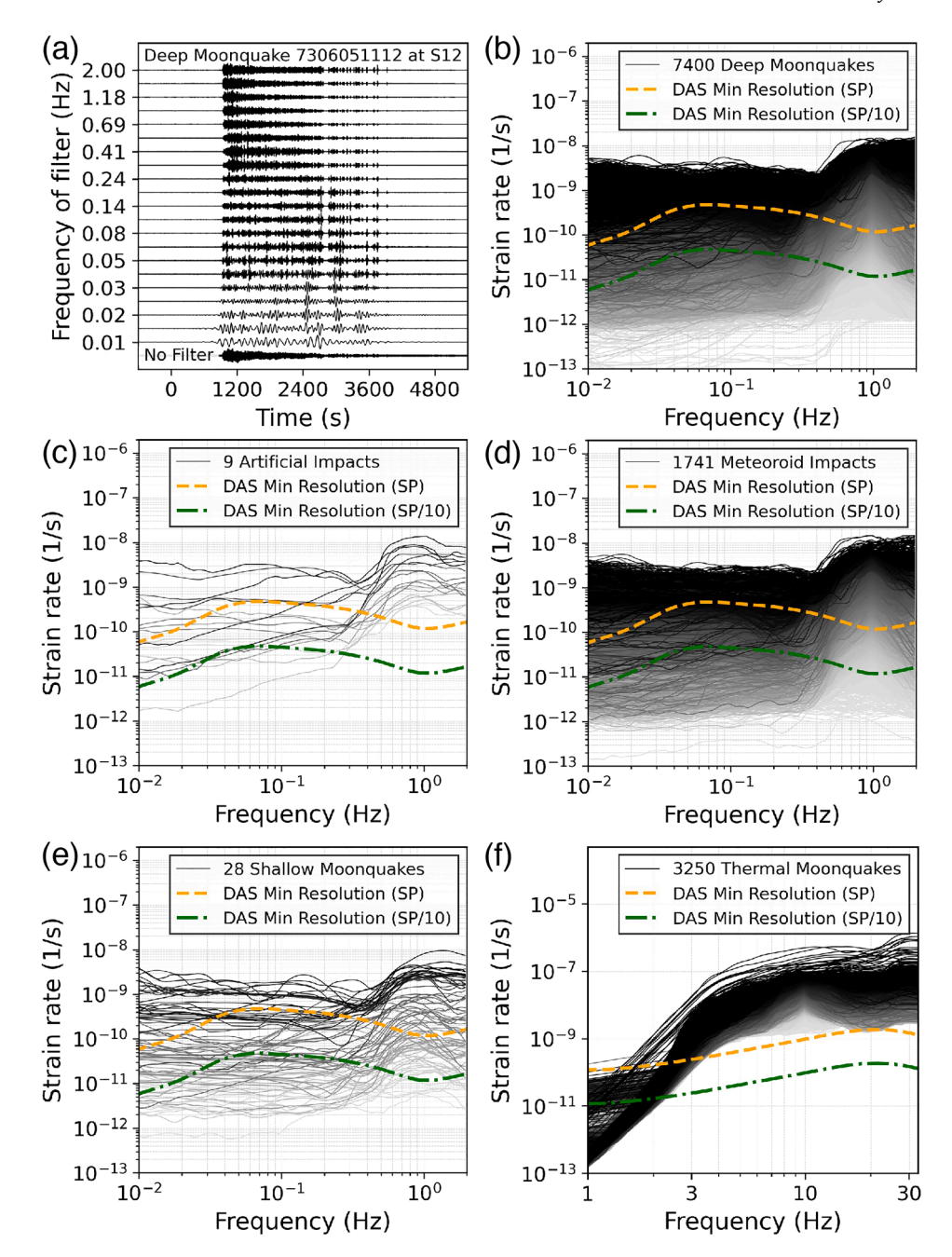


Fig. 7. Comparison of Apollo lunar seismic signals with Earth-based DAS noise level observed at the South Pole of Earth. (a) An example of narrow-band filtering for a deep moonquake recorded by the Apollo 12 seismometer on June 5, 1973, 11:12 UTC. Each band is normalized for visualization. (b-f) Frequency-amplitude plot for octave-wide band-passes of moonquake signals as shown in (a). Each line represents a trace of the waveform of a moonquake. It is colored by its value at 1 Hz (b-e) or 10 Hz (f) for visualization. A darker color means a higher amplitude. The yellow line is the noise level of the South Pole DAS. The green line is an example of reasonable improvement to DAS technology within the next few years whose noise level is assumed 10 times lower than the current South Pole DAS.

4. Results

Fig. 7 shows the spectral analysis results for all moonquakes examined. The data in Fig. 7b-e were recorded by the PSE seismometers, while the data in Fig. 7f were recorded by the LSPE geophones, explaining the varied frequency ranges. Despite the differing origins of the seismic signals, they all exhibit similar spectral signatures. This indicates that the seismometers had a very narrow band of frequencies that they were sensitive to detect, and despite removing the instrument response, only responded to accelerations in that small bandwidth. Notably, the geophones likely did not capture the deep moonquakes and meteoroid impacts recorded by the seismometers during the active periods of LSPE. This suggests that geophones required significantly larger

signal magnitudes at high frequencies for detection, akin to those from local thermal moonquakes (Fig. 7f). These observations suggest that DAS may have the capability to record seismic signals across a broader frequency range than the Apollo instruments (Paitz et al., 2021). However, the comparison in this study is constrained by the limited frequency response of the original Apollo seismometer data.

Fig. 8 and Table 1 summarize analytical outcomes from Fig. 7. Our results show that more than 60 % of the seismic signals recorded by the Apollo seismometers have peak amplitudes that DAS can detect (Fig. 8). Potential improvements to the DAS system—specifically to the laser and cabling—could enhance detection rates significantly. A 10-fold increase in sensitivity, in line with advances documented in existing DAS studies (Han et al., 2021), might enable DAS to detect nearly all moonquakes

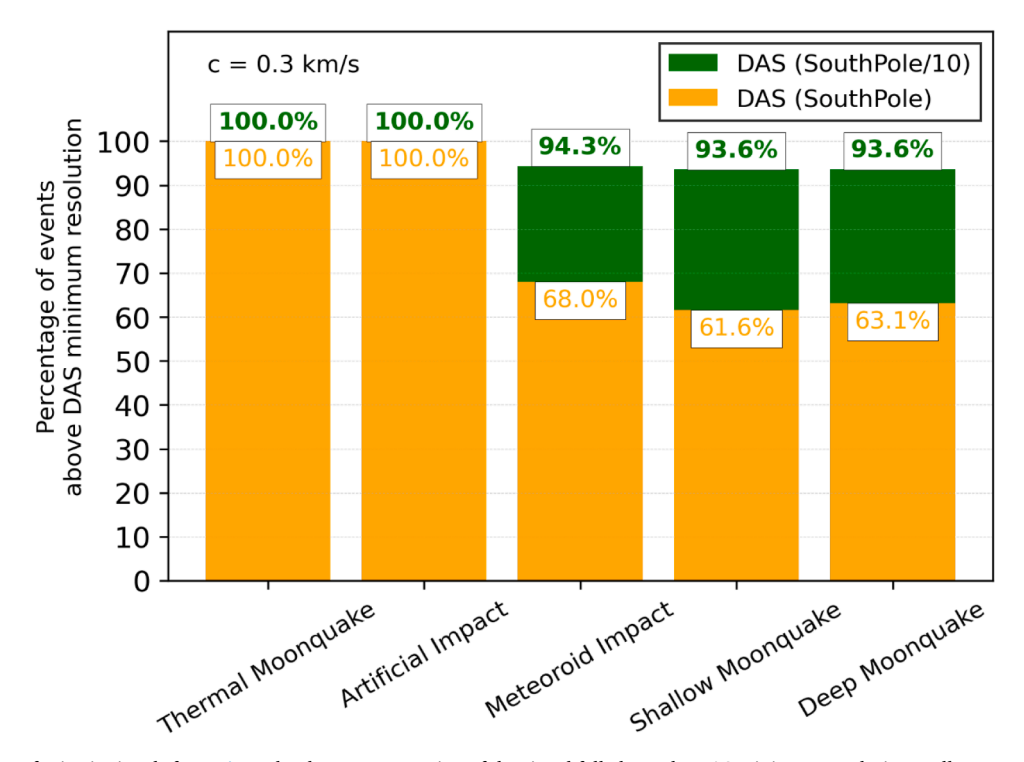


Fig. 8. The percentage of seismic signals from Fig. 7 that have some portion of the signal fall above the DAS minimum resolution. Yellow means the results based on the current South Pole DAS. Green means the results are based on an example of reasonable improvement to DAS technology within the next few years whose noise level is assumed 10 times lower than the current South Pole DAS.

Table 1The expected rates of moonquakes and the percentages of moonquakes above the DAS minimum resolution.

Label Type	Min Rate (events/day)	Max Rate (events/day)	Mean Rate (events/day)	Percentage above SouthPole (%)	Percentage above SouthPole/10 (%)
Thermal Moonquake	0	62	12.811	100	100
Artificial Impact	0	1	0.002	100	100
Meteoroid Impact	0	8	0.405	68.0	94.3
Shallow Moonquake	0	1	0.010	61.6	93.6
Deep Moonquake	0	18	1.643	63.1	93.6

previously observed. Furthermore, Table 1 provides a projection of the number of moonquakes detectable per Earth day using Apollo's seismic data as a reference. With the current DAS technology, at least one deep moonquake would be detectable daily on average, with this number possibly increasing to around eleven (63 % of a maximum of 18 moonquakes/day = 11 moonquakes, Table 1) during the moon's perigee phase, where the likelihood of deep moonquakes is higher.

5. Discussion

Our results affirm that DAS has the capacity to detect moonquakes, providing valuable data on their occurrence over time for different moonquake types. A recent study by Wu et al. (2024) found that a longer DAS cable, which offers more channels for waveform stacking, significantly improves the signal-to-noise ratio. This is particularly beneficial for identifying reflective wave phases such as ScS waves at the core-mantle boundary of the Moon. We explored a range of DAS deployment scenarios on the Moon, as depicted in Fig. 9. These scenarios consider various combinations of operational durations and cable lengths to demonstrate the potential research outcomes under each condition. Notably, we excluded the scenario involving a short operational duration with a long cable. The reason behind this exclusion is grounded in practical considerations: the substantial expense associated with deploying a long cable does not justify its use for only a brief period. This decision underscores the importance of balancing the

cost-effectiveness and scientific value in planning lunar DAS missions. In addition, some curvature in the cable deployment or line segments of varying orientation could be advantageous for signal back-azimuth estimation.

In the short term, the most feasible scenario involves a short DAS cable over a brief period (star A in Fig. 9). A relatively short cable on the order of hundreds of meters will provide the equivalent of more than 100 seismometers in fine spacing. A cable of this length could easily be deployed by astronauts as part of the Artemis missions or by robots (McGarey et al., 2022). There are many thermal moonquakes, especially during temperature changes in lunar sunrise and sunset (Civilini et al., 2023). Tens of thermal events should be detectable within a few Earth days. If the deployment is at the height of thermal seismicity, there will be more than 100 thermal moonquakes detected. It also makes it feasible to determine the source location of the thermal moonquakes in the regolith, something the Apollo 17 four-geophone array could not achieve (Civilini et al., 2023). The data will also allow for the study of the local shallow structure (e.g., regolith, crater, and faults).

Expanding the operation time while maintaining a shorter cable length (star B in Fig. 9). will allow the capture of both deep and superficial thermal moonquakes. This setup is crucial for examining the temporal patterns of moonquakes and could provide insights into the mechanisms of thermal moonquakes. There are currently a few theories of how temperature changes cause moonquakes such as boulder fracturing (Molaro et al., 2017) and differential expansion and contraction

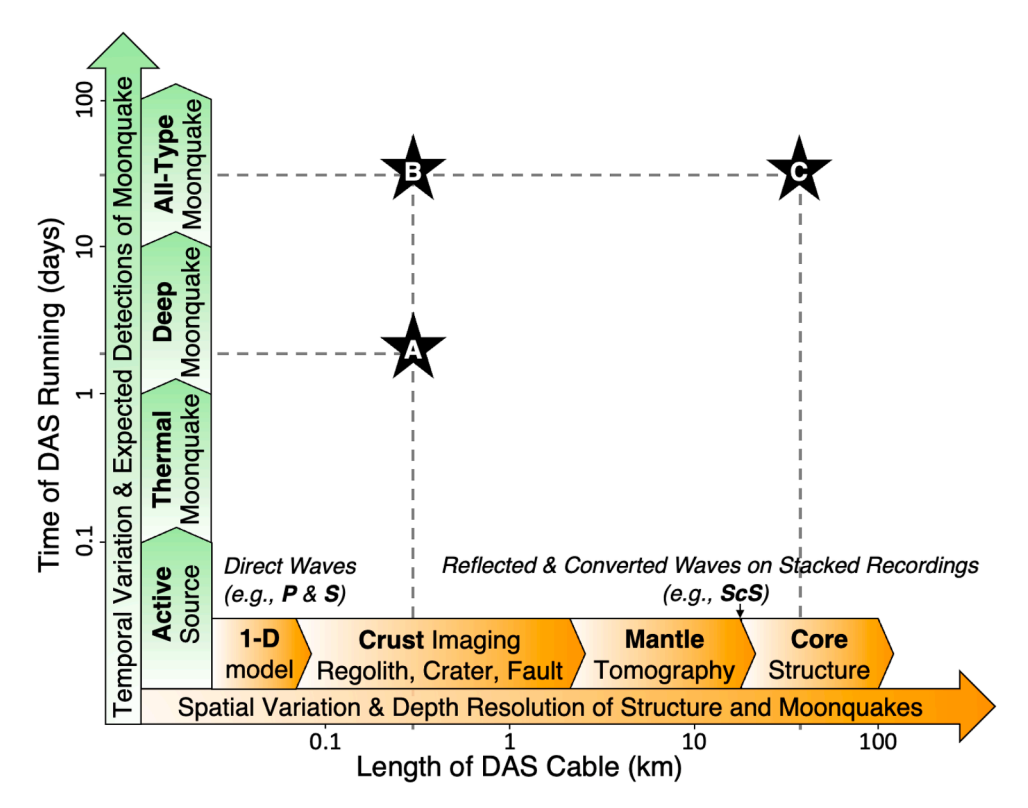


Fig. 9. Schematic diagram representing the correlations between the detectability of moonquakes and the imaging capabilities for lunar structures with the operational duration and the length of the DAS cable used in future lunar experiments. Three distinct scenarios are denoted by stars A, B, and C. Each represents varying combinations of experiment duration and cable length as detailed in the Discussion section.

of minerals within the regolith (Duennebier, 1976). Another benefit of longer-duration catalogs is the ability to do seismic noise correlation across the DAS cable allowing for very detailed velocity models below the array (Yang et al., 2022a). This was previously done with the Apollo 17 mini geophone array, which gave a 1D velocity model down to a 10 m depth (Sens-Schönfelder and Larose, 2010). This type of study would also be able to identify local structures from impact craters and even potential lava tubes that may be used to house future moon bases. However, the study will be limited to areas near the cable.

The most scientifically advantageous but challenging scenario is a long-term deployment featuring an extended cable (star C in Fig. 9). Wu et al. (2024) found that cables longer than 10 km are necessary to measure core phases that allow for an understanding of core structure. Such a comprehensive deployment could facilitate an in-depth analysis of the core, as well as local and regional structures, potentially revealing the nature of impact craters and lava tubes, which are of interest for future lunar habitation.

6. Conclusion

Our results show that DAS is uniquely suited to measure moonquakes in highly scattered environments with low seismic velocity near the moon's surface. Conventional seismometers or even mini arrays of seismometers cannot track the seismic wavefield in that environment as well as DAS. Utilizing DAS noise data from Antarctica as a proxy, we found that DAS can detect all thermal moonquakes that have been previously detected on Apollo 17 geophones. DAS is also able to detect 60 % of the meteoroid impacts and moonquakes that were recorded on all the Apollo seismometers. With achievable and expected improvements in DAS equipment, the detection percentage is expected to improve to over 90 %. We also show that with existing DAS technology, an average of approximately 15 moonquakes daily can be detected, though this number greatly varies during lunar sunrise/sunset and the moon's distance from perigee/apogee. DAS in lunar seismology will be a

significant advancement in the ability to analyze the wave propagation on the moon, which will lead to an important understanding of the moon's interior, marking a transformative step forward in lunar geological studies.

CRediT authorship contribution statement

Qiushi Zhai: Writing – review & editing, Writing – original draft, Visualization, Methodology, Investigation, Formal analysis, Data curation, Conceptualization. Allen Husker: Writing – review & editing, Writing – original draft, Supervision, Resources, Funding acquisition, Data curation, Conceptualization. Zhongwen Zhan: Writing – review & editing, Supervision, Resources, Funding acquisition, Data curation, Conceptualization. Ettore Biondi: Writing – review & editing, Methodology, Investigation, Formal analysis. Jiuxun Yin: Writing – review & editing, Methodology, Investigation, Formal analysis. Francesco Civilini: Writing – review & editing, Data curation. Luis Costa: Writing – review & editing.

Declaration of competing interest

The authors declare that they have no known competing financial interests or personal relationships that could have appeared to influence the work reported in this paper.

Data Availability

The seismic data from Apollo 11-16 are available in the electronic supplementary material from Nunn et al. (2020). The seismic data from the Apollo 17 geophones is published in a CaltechData repository (Civilini, 2023). The image of the lunar near side presented in Fig. 1 can be found on the NASA website at https://moon.nasa.gov/resources/127/lunar-near-side/.

Acknowledgment

This study is supported by the United States National Science Foundation (NSF, grant number EAR-1848166), the United States Geological Survey (USGS, grant number G23AP00111), the Gordon and Betty Moore Foundation, and the Braun Trust. A portion of this research was carried out at the Jet Propulsion Laboratory, California Institute of Technology, under a contract with the National Aeronautics and Space Administration (80NM0018D0004).

Supplementary materials

Supplementary material associated with this article can be found, in the online version, at doi:10.1016/j.epsl.2024.118695.

References

- Ajo-Franklin, J.B., Dou, S., Lindsey, N.J., Monga, I., Tracy, C., Robertson, M., Rodriguez Tribaldos, V., Ulrich, C., Freifeld, B., Daley, T., Li, X., 2019. Distributed acoustic sensing using dark fiber for near-surface characterization and broadband seismic event detection. Sci. Rep. 9, 1328. https://doi.org/10.1038/s41598-018-36675-8.
- Anthony, R.E., Ringler, A.T., DuVernois, M., Anderson, K.R., Wilson, D.C., 2021. Six decades of seismology at South Pole, Antarctica: current limitations and future opportunities to facilitate new geophysical observations. Seismol. Res. Lett. 92, 2718–2735. https://doi.org/10.1785/0220200448.
- Atterholt, J., Zhan, Z., Yang, Y., 2022. Fault zone imaging with distributed acoustic sensing: body-to-surface wave scattering. J. Geophys. Res. 127 https://doi.org/
- Biondi, E., 2021. Target-oriented elastic full-waveform inversion. Stanford Univ. htt ps://web.stanford.edu/group/radar/people/ettore_thesis.pdf.
- Biondi, E., Zhu, W., Li, J., Williams, E.F., Zhan, Z., 2023. An upper-crust lid over the Long Valley magma chamber. Sci. Adv. 9, eadi9878. https://doi.org/10.1126/sciadv.adi9878
- Blanchette-Guertin, J.-F., Johnson, C.L., Lawrence, J.F., 2012. Investigation of scattering in lunar seismic coda. J. Geophys. Res. 117 https://doi.org/10.1029/ 2011JE004042.
- Bulow, R.C., Johnson, C.L., Shearer, P.M., 2005. New events discovered in the Apollo lunar seismic data. J. Geophys. Res. 110 https://doi.org/10.1029/2005JE002414.
- Civilini, F., 2023. Apollo 17 lunar seismic profiling experiment seismic data and thermal moonquake catalog. https://doi.org/10.22002/gc871-q2a25.
- Civilini, F., Weber, R., Husker, A., 2023. Thermal moonquake characterization and cataloging using frequency-based algorithms and stochastic gradient descent. J. Geophys. Res. 128, e2022JE007704 https://doi.org/10.1029/2022JE007704.
- Civilini, F., Weber, R.C., Jiang, Z., Phillips, D., Pan, W.D., 2021. Detecting moonquakes using convolutional neural networks, a non-local training set, and transfer learning. Geophys. J. Int. 225, 2120–2134. https://doi.org/10.1093/gji/ggab083.
- Clinton, J.F., Heaton, T.H., 2002. Potential advantages of a strong-motion velocity meter over a strong-motion accelerometer. Seismol. Res. Lett. 73, 332–342. https://doi. org/10.1785/gssrl.73.3.332.
- Cohen, B.A., 2020. Lunar mission priorities for the decade 2023–2033, https://ntrs.nasa.gov/api/citations/20205003736/downloads/Barbara%20Cohen_%20LEAG% 20Mission%20Priorities%20White%20Paper.pdf.
- Cooper, M.R., Kovach, R.L., 1975. Energy, frequency, and distance of moonquakes at the Apollo 17 site. In: Lunar and Planetary Science Conference Proceedings, pp. 2863–2879.
- Cooper, M.R., Kovach, R.L., Watkins, J.S., 1974. Lunar near-surface structure. Rev. Geophys. 12, 291–308. https://doi.org/10.1029/RG012i003p00291.
- Dainty, A.M., Toksöz, M.N., Anderson, K.R., Pines, P.J., Nakamura, Y., Latham, G., 1974.
 Seismic scattering and shallow structure of the Moon in Oceanus Procellarum. Moon
 9, 11–29.
- Duennebier, F., 1976. Thermal movement of the regolith, in: in: lunar Science Conference, 7th, Houston, Tex., March 15-19, 1976, Proceedings. Volume 1.(A77-34651 15-91) New York, Pergamon Press, Inc., 1976, p. 1073–1086. pp. 1073–1086.
- Duennebier, F., Sutton, G.H., 1974. Thermal moonquakes. J. Geophys. Res. 79, 4351–4363. https://doi.org/10.1029/JB079i029p04351 (1896-1977).
- Garcia, R.F., Khan, A., Drilleau, M., Margerin, L., Kawamura, T., Sun, D., Wieczorek, M. A., Rivoldini, A., Nunn, C., Weber, R.C., Marusiak, A.G., Lognonné, P., Nakamura, Y., Zhu, P., 2019. Lunar seismology: an update on interior structure models. Space Sci. Rev. 215, 50. https://doi.org/10.1007/s11214-019-0613-y.
- Gillet, K., Margerin, L., Calvet, M., Monnereau, M., 2017. Scattering attenuation profile of the Moon: implications for shallow moonquakes and the structure of the megaregolith. Phys. Earth Planetary Interiors 262, 28–40. https://doi.org/10.1016/ i.pepi.2016.11.001.
- Goins, N.R., Dainty, A.M., Toksöz, M.N., 1981. Lunar seismology: the internal structure of the Moon. J. Geophys. Res. 86, 5061–5074. https://doi.org/10.1029/ JB086iB06p05061.
- Haase, I., Wählisch, M., Gläser, P., Oberst, J., Robinson, M.S., 2019. Coordinates and Maps of the Apollo 17 Landing Site. Earth Space Sci. 6, 59–95. https://doi.org/ 10.1029/2018EA000408.
- Han, B., Guan, H., Yao, J., Rao, Y.-J., Ran, Z., Gong, Y., Li, Q., Li, M., Zhang, R., An, S., Yu, G., Wang, X., 2021. Distributed acoustic sensing with sensitivity-enhanced

- optical cable. IEEE Sens. J. 21, 4644–4651. https://doi.org/10.1109/ JSEN 2020 3035002
- Haviland, H.F., Weber, R.C., Neal, C.R., Lognonné, P., Garcia, R.F., Schmerr, N., Nagihara, S., Grimm, R., Currie, D.G., Dell'Agnello, S., Watters, T.R., Panning, M.P., Johnson, C.L., Yamada, R., Knapmeyer, M., Ostrach, L.R., Kawamura, T., Petro, N., Bremner, P.M., 2022. The lunar geophysical network landing sites science rationale. Planet. Sci. J. 3, 40. https://doi.org/10.3847/PSJ/ac0f82.
- Heffels, A., Knapmeyer, M., Oberst, J., Haase, I., 2017. Re-evaluation of Apollo 17 Lunar Seismic Profiling Experiment data. Planet Space Sci. 135, 43–54. https://doi.org/ 10.1016/j.pss.2016.11.007.
- Jeon, I., Ahn, C., Kim, C., Park, S., Jeon, W., Duan, L., Kim, J., 2023. Palm-sized, vibration-insensitive, and vacuum-free all-fiber-photonic module for 10–14-level stabilization of CW lasers and frequency combs. APL. Photonics. 8, 120804 https://doi.org/10.1063/5.0160834.
- Jousset, P., Currenti, G., Schwarz, B., Chalari, A., Tilmann, F., Reinsch, T., Zuccarello, L., Privitera, E., Krawczyk, C.M., 2022. Fibre optic distributed acoustic sensing of volcanic events. Nat. Commun. 13, 1753. https://doi.org/10.1038/s41467-022-29184-w.
- Kawamura, T., Grott, M., Garcia, R., Wieczorek, M., de Raucourt, S., Lognonné, P., Bernauer, F., Breuer, D., Clinton, J., Delage, P., Drilleau, M., Ferraioli, L., Fuji, N., Horleston, A., Kletetschka, G., Knapmeyer, M., Knapmeyer-Endrun, B., Padovan, S., Plesa, A.-C., Rivoldini, A., Robertsson, J., Rodriguez, S., Stähler, S.C., Stutzmann, E., Teanby, N.A., Tosi, N., Vrettos, C., Banerdt, B., Fa, W., Huang, Q., Irving, J., Ishihara, Y., Miljković, K., Mittelholz, A., Nagihara, S., Neal, C., Qu, S., Schmerr, N., Tsuji, T., 2022. An autonomous lunar geophysical experiment package (ALGEP) for future space missions. Exp. Astron. 54, 617–640. https://doi.org/10.1007/s10686-022-09857-6.
- Kennett, B.L.N., Furumura, T., 2013. High-frequency Po/So guided waves in the oceanic lithosphere: i—long-distance propagation. Geophys. J. Int. 195, 1862–1877. https://doi.org/10.1093/gji/ggt344.
- Kovach, R.L., Watkins, J.S., 1973. Apollo 17 seismic profiling: probing the lunar crust. Science (1979) 180, 1063–1064. https://doi.org/10.1126/science.180.4090.1063.
- Kovach, R.L., Watkins, J.S., Talwani, P., 1973. Lunar seismic profiling experiment, in Apollo 17— Preliminary Science Report. NASA SP-330. https://ntrs.nasa.gov/citations/19740010315.
- Lammlein, D.R., Latham, G.V., Dorman, J., Nakamura, Y., Ewing, M., 1974. Lunar seismicity, structure, and tectonics. Rev. Geophys. 12, 1–21. https://doi.org/ 10.1029/RG012i001p00001.
- Larose, E., 2005. Lunar subsurface investigated from correlation of seismic noise. Geophys. Res. Lett. 32 https://doi.org/10.1029/2005gl023518.
- Latham, G.V., Ewing, M., Press, F., Suttorn, G., Dorman, J., Nakamura, Y., Toksoz, N., Duennebier, F., Lammlein, D., 1971. Passive seismic experiment, in Apollo 14—Preliminary Science Report. NASA SP-272. https://ntrs.nasa.gov/citations/19 710021477
- Li, J., Kim, T., Lapusta, N., Biondi, E., Zhan, Z., 2023. The break of earthquake asperities imaged by distributed acoustic sensing. Nature 1–7. https://doi.org/10.1038/ s41586-023-06227-w.
- Lindsey, N.J., Martin, E.R., 2021. Fiber-optic seismology. Annu. Rev. Earth Pl Sc 49, 309–336. https://doi.org/10.1146/annurev-earth-072420-065213.
- Lognonné, P., Banerdt, W.B., Clinton, J., Garcia, R.F., Giardini, D., Knapmeyer-Endrun, B., Panning, M., Pike, W.T., 2023. Mars seismology. Annu. Rev. Earth Planet Sci. 51 https://doi.org/10.1146/annurev-earth-031621-073318 null.
- Martin, E.R., Castillo, C.M., Cole, S., Sawasdee, P.S., Yuan, S., Clapp, R., Karrenbach, M., Biondi, B.L., 2017. Seismic monitoring leveraging existing telecom infrastructure at the SDASA: active, passive, and ambient-noise analysis. Leading Edge 36, 1025–1031. https://doi.org/10.1190/tle36121025.1.
- McAllister, B.D., Kerr, J., Zimmer, J., Kovach, R.L., Watkins, J., 1969. A seismic refraction system for lunar use. IEEE Trans. Geosci. Electron. 7, 164–171. https://doi.org/10.1109/TGE.1969.271374.
- McGarey, P., Nesnas, I.A., Rajguru, A., Bezkrovny, M., Jamnejad, V., Lux, J., Sunada, E., Teitelbaum, L., Miller, A., Squyres, S.W., Hallinan, G., Hegedus, A., Burns, J.O., 2022. How to deploy a 10-km interferometric radio telescope on the moon with just four tethered robots. In: 2022 IEEE Aerospace Conference (AERO), pp. 1–8. https://doi.org/10.1109/AERO53065.2022.9843745.
- Molaro, J.L., Byrne, S., Le, J.-L., 2017. Thermally induced stresses in boulders on airless body surfaces, and implications for rock breakdown. Icarus 294, 247–261. https:// doi.org/10.1016/j.icarus.2017.03.008.
- Nakamura, Y., 2005. Farside deep moonquakes and deep interior of the Moon. J. Geophys. Res. 110 https://doi.org/10.1029/2004JE002332.
- Nakamura, Y., Latham, G.V., Dorman, H.J., Harris, J.E., 1981. Passive seismic experiment, long period event catalog, final version (1969 Day 202 - 1977 Day 273, ALSEP Stations 11, 12, 13, 14, 15, and 16) (Technical Report). Inst. Geophys. https://doi.org/10.15781/TZFF3MH78.
- Nielsen, L., Thybo, H., 2006. Identification of crustal and upper mantle heterogeneity by modelling of controlled-source seismic data. Tectonophys., Heterogeneous Mantle 416, 209–228. https://doi.org/10.1016/j.tecto.2005.11.020.
- Nunn, C., Garcia, R.F., Nakamura, Y., Marusiak, A.G., Kawamura, T., Sun, D., Margerin, L., Weber, R., Drilleau, M., Wieczorek, M.A., Khan, A., Rivoldini, A., Lognonné, P., Zhu, P., 2020. Lunar seismology: a data and instrumentation review. Space Sci. Rev. 216 https://doi.org/10.1007/s11214-020-00709-3.
- Nunn, C., Pike, W.T., Calcutt, S.B., Standley, I.M., Kedar, S., Weber, R.C., Neal, C.R., Panning, M.P., 2019. Standing on apollo's shoulders: MEMS seismometers for the lunar geophysical network. In: AGU Fall Meeting Abstracts, pp. P33D–P308.
- Ogden, H.M., Murray, M.J., Murray, J.B., Kirkendall, C., Redding, B., 2021. Frequency multiplexed coherent ϕ -OTDR. Sci. Rep. 11, 17921. https://doi.org/10.1038/s41598-021-97647-z.

- Paitz, P., Edme, P., Graff, D., Walter, F., Doetsch, J., Chalari, A., Schmelzbach, C., Fichtner, A., 2021. Empirical investigations of the instrument response for distributed acoustic sensing (DAS) across 17 Octaves. B Seismol. Soc. Am. 111, 1–10. https://doi.org/10.1785/0120200185.
- Panning, M., Kedar, S., Bowles, N., Calcutt, S., Cutler, J., Elliott, J., Garcia, R.F., Kawamura, T., Lognonne, P., Miller, E., 2021. Farside Seismic Suite (FSS): first seismic data from the farside of the Moon delivered by a commercial lander. in: AGU Fall Meeting Abstracts P54C–P501.
- Panning, M., Weber, R., Kedar, S., Bugby, D., Calcutt, S., Currie, D., Agnello, S.D., Elliott, J., Grimm, R., Gulick, S., others, 2020. Building a lunar network using a long-lived, human-deployed lunar geophysical package (LGP), https://www.lpi.usra.edu/announcements/artemis/whitepapers/2019.pdf.
- Peterson, J.R., 1993. Observations and modeling of seismic background noise. Open-File Report U.S. Geol. Surv. (93–322). https://doi.org/10.3133/ofr93322.
- Robertsson, J.O.A., 1996. A numerical free-surface condition for elastic/viscoelastic finite-difference modeling in the presence of topography. Geophysics 61, 1921–1934. https://doi.org/10.1190/1.1444107.
- Sens-Schönfelder, C., Larose, E., 2010. Lunar noise correlation, imaging and monitoring. Earthq. Sci. 23, 519–530. https://doi.org/10.1007/s11589-010-0750-6.
- Shearer, C., 2017. Lunar Geophysical Network (LGN), https://solarsystem.nasa.gov/st udies/203/lunar-geophysical-network-lgn.
- Spica, Z.J., Perton, M., Martin, E.R., Beroza, G.C., Biondi, B., 2020. Urban seismic site characterization by fiber-optic seismology. J. Geophys. Res. 125, e2019JB018656 https://doi.org/10.1029/2019JB018656.
- Standley, I.M., Pike, W.T., Calcutt, S., Hoffman, J.P., 2023. Short period seismometer for the lunar Farside seismic suite mission, in: 2023 IEEE Aerospace Conference. Presented at the 2023 IEEE Aerospace Conference, pp. 1–9. https://doi.org/10.110 9/AERO55745.2023.10115559.
- Sutton, G.H., Latham, G.V., 1964. Analysis of a feedback-controlled seismometer.

 J. Geophys. Res. 69, 3865–3882. https://doi.org/10.1029/JZ069i018p03865.
- Toksöz, M.N., Dainty, A.M., Solomon, S.C., Anderson, K.R., 1974. Structure of the Moon. Rev. Geophys. 12, 539–567. https://doi.org/10.1029/RG012i004p00539.
- Turner, A.R., Hawthorne, J.C., Gaddes, M., 2022. Stresses in the lunar interior: insights from slip directions in the A01 deep moonquake nest. J. Geophys. Res. 127, e2022JE007364 https://doi.org/10.1029/2022JE007364.
- Vidal-Moreno, P.J., Rochat, E., Fermoso, P., Fernández-Ruiz, M.R., Martins, H., Martin-Lopez, S., Ocaña, M., Gonzalez-Herraez, M., 2022. Cancellation of reference update-induced 1/f noise in a chirped-pulse DAS. Opt. Lett., OL 47, 3588–3591. https://doi.org/10.1364/OL.465367.
- Walter, F., Gräff, D., Lindner, F., Paitz, P., Köpfli, M., Chmiel, M., Fichtner, A., 2020.Distributed acoustic sensing of microseismic sources and wave propagation in

- glaciated terrain. Nat. Commun. 11, 2436. https://doi.org/10.1038/s41467-020-15824-6
- Watters, T.R., Weber, R.C., Collins, G.C., Howley, I.J., Schmerr, N.C., Johnson, C.L., 2019. Shallow seismic activity and young thrust faults on the Moon. Nat. Geosci. 12, 411–417. https://doi.org/10.1038/s41561-019-0362-2.
- Weber, R.C., Neal, C., Banerdt, B., Beghein, C., Chi, P., Currie, D., Dell'Agnello, S., Garcia, R., Garrick-Bethell, I., Grimm, R., Grott, M., Haviland, H., Kawamura, T., Kedar, S., Lognonné, P., Nagihara, S., Nakamura, Y., Nunn, C., Ostrach, L., Panning, M., Petro, N., Schmerr, N., Siegler, M., Watters, T., Wieczorek, M., Zacny, K., 2020. The lunar geophysical network mission. Presented at the SEG International Exposition and Annual Meeting, OnePetro. https://doi.org/10.1190/segam2020-3416702.1.
- Westbrook, P.S., Kremp, T., Zhu, B., Ko, W., Shi, Z., Feder, K.S., 2023. Enhanced backscatter fibers for sensing in telecom networks. J. Lightwave Technol. 41, 1010–1016. JLT
- Williams, E.F., Fernández-Ruiz, M.R., Magalhaes, R., Vanthillo, R., Zhan, Z., González-Herráez, M., Martins, H.F., 2019. Distributed sensing of microseisms and teleseisms with submarine dark fibers. Nat. Commun. 10, 5778. https://doi.org/10.1038/s41467-019-13262-7.
- Wu, W., Zhan, Z., Panning, M., Klesh, A., 2024. Fiber seismic network on the moon. Seismol. Res. Lett. https://doi.org/10.1785/0220230067.
- Yamada, R., Garcia, R.F., Lognonné, P., Feuvre, M.L., Calvet, M., Gagnepain-Beyneix, J., 2011. Optimisation of seismic network design: application to a geophysical international lunar network. Planet. Space Sci. 59, 343–354. https://doi.org/ 10.1016/j.pss.2010.12.007.
- Yang, Y., Atterholt, J.W., Shen, Z., Muir, J.B., Williams, E.F., Zhan, Z., 2022a. Sub-kilometer correlation between near-surface structure and ground motion measured with distributed acoustic sensing. Geophys. Res. Lett. 49 https://doi.org/10.1029/2021g1096503.
- Yang, Y., Zhan, Z., Shen, Z., Atterholt, J., 2022b. Fault zone imaging with distributed acoustic sensing: surface-to-surface wave scattering. J. Geophys. Res. 127 https:// doi.org/10.1029/2022ib024329.
- Yu, C., Zhan, Z., Lindsey, N.J., Ajo-Franklin, J.B., Robertson, M., 2019. The potential of DAS in teleseismic studies: insights from the goldstone experiment. Geophys. Res. Lett. 46, 1320–1328. https://doi.org/10.1029/2018GL081195.
- Zhai, Q., Zhan, Z., Chavarria, J.A., 2024. Thousand-Kilometer DAS Array Reveals an Uncatalogued Magnitude-5 Dynamically Triggered Event After the 2023 Turkey Earthquake. J. Geophys. Res.: Solid Earth 129, e2023JB027680. https://doi.org/ 10.1029/2023JB027680.
- Zhan, Z., 2019. Distributed acoustic sensing turns fiber-optic cables into sensitive seismic antennas. Seismol. Res. Lett. 91, 1–15. https://doi.org/10.1785/0220190112.